Effect of carbon on the oxidation of Fe–5.5Al–0.55C alloy

C. H. KAO, C. M. WAN
Institute of Materials Science and Engineering, National Tsing Hua University, Hsinchu, Taiwan

An alloy with the chemical composition Fe–5.5 wt % Al–0.55 wt % C is employed to investigate the effect of carbon on the oxidation at 600, 800 and 1000° C in dry air. Kinetic curves were determined by thermogravimetry analyses. Optical metallography and electron probe micro-analysis were used to examine the oxide scales formed on the alloy surfaces. The kinetic curves observed at 600, 800 and 1000° C had simple, three-stage and two-stage parabolic rate laws, respectively. No carbide-free layer could be observed in the alloy which was oxidized at 600° C. In contrast, a carbide-free zone was found in specimens of the alloy after oxidizing at 800 and 1000° C.

1. Introduction

It has long been recognized that the addition of a certain amount of aluminium can improve the oxida-tion resistance of some steels by the formation of a protective Al_2O_3 thin film. Mogan and Zackay [1] indicated that Fe–8 wt % Al alloy is equivalent in oxidation resistance to Type 302 18-8 stainless steel. Above this aluminium level the iron–aluminium alloys are superior to most commercial austentic steels and also this superiority increases with increasing service temperature. Unfortunately, when the aluminium content exceeds about 8 wt %, these alloys show poor hot and cold workabilities and also present fabricating difficulties. For the past twenty years, the addition of manganese and carbon was believed to have the capability to reduce these difficulties since both man-ganese and carbon are austenitic stabilizers. Hence a reasonable arrangement of the Fe–Mn–Al–C chemi-cal composition always gives a full austenitic alloy with good mechanical properties and a high oxidation resistance at high temperatures [2–4].

Our recent work [5], which indicates some interest-ing results on the isothermal oxidation behaviour of Fe–Mn–Al–C alloys in air concludes that the rela-tionship between decarburization and oxide scales is much more complicated than expected. This is be-cause the interference of decarburization is harmful to the formation of a continuous film of Al_2O_3. Thus it leads to the decreased high-temperature oxidation resistance of these alloys. In addition, even for a fully austenitic Fe–Mn–Al–C alloy, a thin layer of ferrite is always formed during the initial period of a high-temperature oxidation experiment due to the decrease of carbon and manganese contents in the surface region. Therefore, the formation of oxides on the alloy surface can always be correlated with a newly formed ferrite layer, no matter whether the alloy is originally a fully austenitic steel or not. Thus, in order to gain a more complete understanding of the oxidation mechanism of the Fe–Mn–Al–C system, the present

work was initiated to study the effect of carbon on oxidation resistance by using a simple alloy such as Fe–Al–C. In addition, the correlation of oxidation behaviour and decarburization occurring during oxidation was also investigated.

2. Experimental details

2.1. Alloy fabrication

The alloy used in the present studies was melted in an air induction furnace under a protective argon atmosphere and the chemical composition of the alloys is listed in Table I. Ingots of the alloy were first forged at 1200° C, from 7 to 2.5 cm, and sub-sequently homogenized at 1100° C for 4 h. After surface finishing, the surface and edges of the speci-mens were mechanically polished with abrasive paper up to 1200 grit. Each specimen was degreased with distilled water and finally cleaned ultrasonically in acetone before the oxidation experiment.

2.2. Oxidation experiments

Oxidation experiments for the present study were all performed in the infrared image furnace of an Ulvac/Shink–Uriko thermobalance under a dry air atmosphere with a flow rate of 100 ml min^{-1} and oxi-dation temperatures of 600, 800 and 1000° C. The testing temperature was fixed by an automatic tem-perature controller. The heating and cooling rates of the infrared image furnace were 100° C min^{-1}. The oxidation temperature and weight gain curves of the test specimen were recorded by a chart recorder.

2.3. Analysis

The phases present in specimens were identified with X-ray diffraction using a copper target with a nickel filter and a graphite single-crystal monochromator. The morphology of the oxide scale was examined by optical microscopy.

The elemental redistribution and concentration profile in the oxidized specimens were characterized

TABLE I Chemical composition of the tested alloy

Element	Al	C	Mn	Si	P	S	Fe
Composition (wt %)	5.51	0.55	0.01	0.02	0.01	0.021	Bal.

by electron probe microanalysis (EPMA) (Jeol JCXA-733). Quantitative analysis of iron and aluminium was performed with the aid of a ZAF-corrected program. The operation of EPMA was carried out by first raising the voltage to 25 kV with probe current 0.03 μA.

3. Experimental results

3.1. Characteristics of alloy before oxidation

Fe–5.5 Al–0.55 C alloy after hot forging and 4 h homogenization at 1100° C was found by X-ray diffraction to be a two-phase material with iron–aluminium carbide (Fe_3AlC_x) in the ferrite matrix. The lattice parameters were 0.287 and 0.377 nm for ferrite and carbide, respectively. Fig. 1 shows the microstructure in this condition. The dark areas in the micrograph are iron–aluminium carbide particles (Fe_3AlC_x), whereas light areas are the ferrite region.

3.2. Oxidation kinetics

In order to achieve a better understanding of the correlation of temperature and the oxidation behaviour of iron–aluminium–carbon alloy, oxidation experiments were carried out at three different temperatures of 600, 800 and 1000° C. Plots of weight gain per unit area as a function of oxidation time and temperature are shown in Fig. 2 for the present alloy. It was observed that the weight gain increased with increasing temperature in the oxidation experiments; Figs 3a, b and c show the square of the weight gain per unit area against time for the alloy at 600, 800 and 1000° C, respectively. It was found that there is a straight-line relationship for the oxidation at 600° C, indicating that the oxidation behaviour follows a simple parabolic rate law at this temperature. The evaluated value of the parabolic constant, k_p1, is 1.6×10^{-10} $g^2 cm^{-4} sec^{-1}$.

Oxidation kinetics obtained from the experiments carried out at 800 and 1000° C appeared to be different from the one carried out at 600° C. As shown in Figs
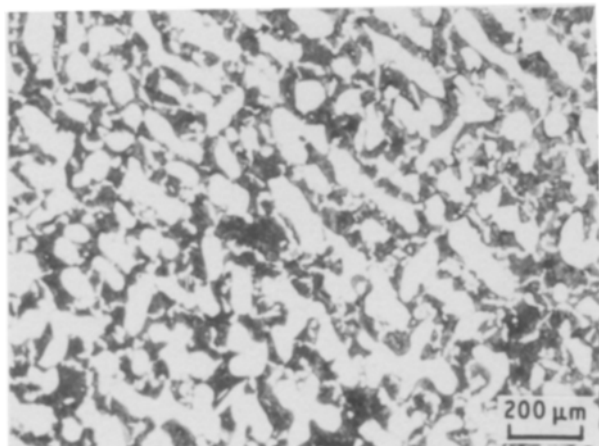
TABLE II Parabolic rate constants for the oxidation of Fe–5.5 Al–0.55 C alloy

Temperature (°C)	Rate constant ($g^2 cm^{-4} sec^{-1}$)		
	k_p1	k_p2	k_p3
600	1.63×10^{-10}	–	–
800	2.1×10^{-10} (<3 h)	5.7×10^{-10} (3 to 10 h)	3.6×10^{-10} (10 to 24 h)
1000	6.27×10^{-9} (<5 h)	–	7.3×10^{-11} (10 to 24 h)

3b and c, the kinetic result at 800° C had three distinct parabolic rates and that at 1000° C had two distinct parabolic rates for the present alloy. All the parabolic rate constants were calculated and are listed in Table II. The reproducibility of each kinetic curve was checked and had a very slight fluctuation, approximately ± 2%. From the oxidation behaviour of the present alloy at 800° C, the initial rate constant (referred to as k_p1) is the lowest and generally lasts for 3 h. The second rate constant (k_p2) has the highest value among the three distinct parabolic rate constants and it generally lasts for about 3 to 13 h. During the final stage, the third rate constant (k_p3) is slightly lower than the second rate constant.

Fig. 3c shows two distinct parabolic rates at 1000° C. The initial parabolic rate constant (k_p1) is higher than the final parabolic rate constant (k_p2) and generally lasts for 4 or 5 h, after which oxidation is at the second oxidation stage with a parabolic rate constant k_p2. Table II indicates that initial parabolic rate constant of the present alloy increased with increasing temperature in the oxidation experiments. In contrast, the lowest value of the last parabolic rate constant was found to be at the oxidation temperature of 1000° C.

3.3. Analytical aspects

An examination of the cross-section of an oxidized specimen after 24 h oxidation at 600° C is shown in Fig. 4, which indicates that there are two clearly evident oxide layers with a porous exterior. No carbide-free layer can be observed in this condition. Observation by an X-ray mapping technique shows that there are two oxide layers rich in iron. However, the oxide–matrix interface was found to be rich in
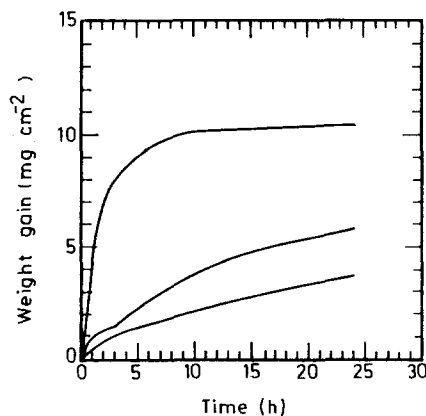

Figure 1 Fe–5.5 Al–0.55 C microstructure after heat treatment (4 h at 1100° C).

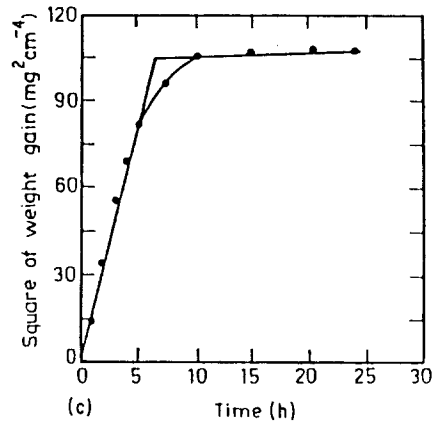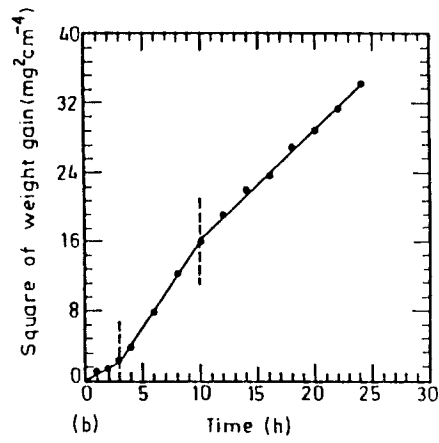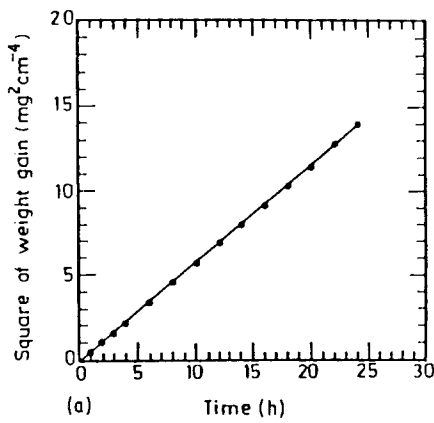*Figure 2* Thermogravimetric oxidation curves of Fe–5.5 Al–0.55 C alloy at different temperatures.

(a)

(b)

(c)

Figure 3 The square of weight gain per unit area against time for Fe–5.5 Al–0.55 C alloy at (a) 600, (b) 800, (c) 1000° C.

aluminium. Fig. 5 shows the concentration of elements in these layers and in the matrix, determined by an electron microprobe with a line scanning profile technique.

The metallographic appearance of the cross-section of the 24 h oxidized alloy with oxidation temperature 800° C indicates the existence of many nodules. Fig. 6a reveals the ellipsoidal shape of these nodules. Fig. 6b shows the concentration profile from the outside scale to the inside matrix, corresponding to Fig. 6a. From these two figures, the upper half of the nodules was identified as being rich in iron, but had a negligible amount of aluminium. The lower region had a higher aluminium concentration of about 8 wt % The aluminium concentration increases to a value of about 16.7 wt % in the region close to the alloy–oxide interface. No internal oxide could be observed.
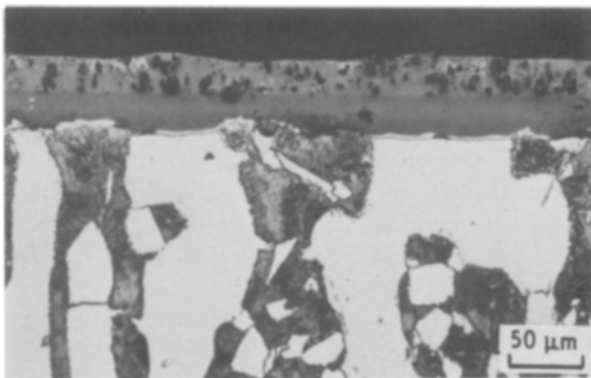
Through optical microstructure investigation, no

iron–aluminium carbide could be seen in specimens oxidized for 10 h at 800° C. In addition, according to line profile analysis using Auger electron spectroscopy, no carbon was detected in this condition.

Oxide nodules, which were found on the surface of specimen after oxidation, were mostly randomly distributed, but a higher density of nodules was observed along grain boundaries and at specimen corners. The size of the nodules increased with increasing oxidation time.

Fig. 7 shows that the specimen surface of the present alloy was covered by many oxide nodules after one hour of oxidation at 1000° C. Through optical investigation, no carbides could be observed. Fig. 8a shows a scanning electron micrograph of the oxide scale formed after 2 h oxidation at 1000° C. According to X-ray mapping (Figs 8b, c and d) the highest aluminium concentration was found along the oxide–matrix interface. Optical morphology studies indicated that the oxides formed after more than 12 h oxidation were similar to those formed after just twelve hours. Fig. 9a shows the metallographic structure of a cross-section of the oxide scale formed after 24 h oxidation at 1000° C. The concentration profile across the line marked in Fig. 9a is shown in Fig. 9b. It indicates that the outer oxide scale was rich in iron. The aluminium concentration in the scale increased more towards the oxide–matrix interface.

Figure 4 Metallographic cross-section of the oxide scale on Fe–5.5 Al–0.55 C alloy after 24 h at 600° C.
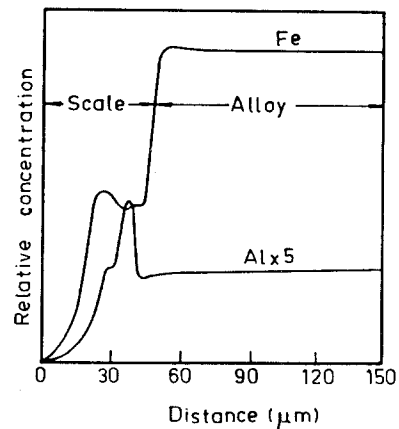

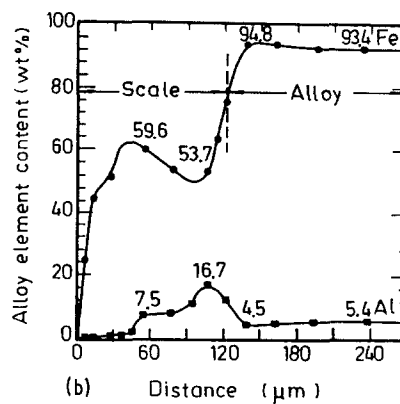*Figure 5* Line scanning profile of the oxide scale on Fe–5.5 Al–0.55 C alloy after 24 h at 600° C.
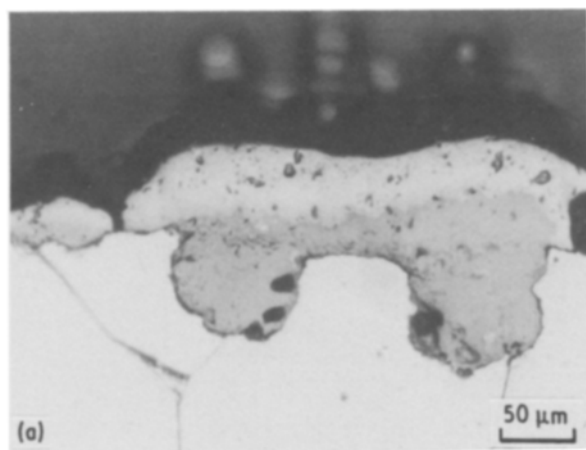
3205

Figure 6 (a) Metallographic cross-section of nodules on Fe–5.5 Al–0.55 C after 24 h at 800° C. (b) The concentration profile across scale and adjoining alloy (line of traverse in (a)).

4. Discussion

According to the results of kinetic studies, the carbon content of the alloy used in the present study (0.55 wt % C plus Fe–5.5 Al) had a harmful effect on the high-temperature oxidation resistance in comparison with a previous report [6]. This indicates that carbon in the alloy always increases the rate of oxidation of Fe–Al alloy. Similar results were also reported by Boggs [7], who concluded that the oxidation rate of Fe–Al–C alloys increased with increasing carbon concentration at 800° C. Our results demonstrated that the oxidation kinetics of the alloy followed a parabolic law, suggesting that the oxidation was controlled by a diffusion mechanism. It is interesting to note, however, that three different kinds of oxidation behaviour were observed at different oxidation temperatures in this study.

Fig. 3a indicates that the present alloy follows a simple parabolic rate law at 600° C. A metallographic cross-section of the oxide scale on Fe–5.5 Al–0.55 C alloy after 24 h at 600° C is shown in Fig. 4. No carbide-free layer could be observed in the alloy under such conditions. All these facts suggest that the outward diffusion elemental carbon is not quick enough to form a continuous carbide-free layer between the oxide scales and the matrix during the oxidation exp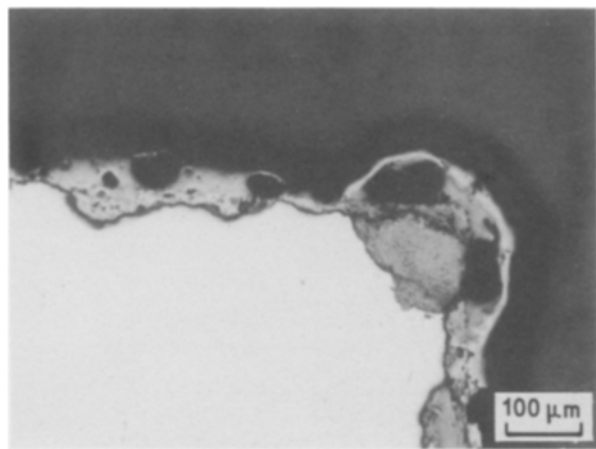eriment at 600° C. It seems that the effect of carbon on the oxidation behaviour of the alloy is only closely correlated with decomposition along the oxide–matrix interface in such conditions. CO or CO_2 that is formed by the carbon atoms produced by the decomposition of carbide and oxygen diffusing in from the outside may diffuse out through the scales via pores and microcracks, which results in the lower oxidation resistance of the present alloy compared with Fe–Al alloy.

According to the combination of optical morphology, X-ray mapping and the X-ray diffraction investigations of the surfaces of the oxidized specimens with different depths, the oxide scale of the present alloy oxidized at 600° C consisted of a porous layer of Fe_2O_3 and Fe_3O_4. There was also an inner layer of $FeFe_xAl_{2-x}O_4$ ($0 \leqslant x \leqslant 2$) along the scale–metal interface.

The oxide formation mechanism of the present alloy at 600° C was suggested as follows. The initial stage of oxidation is characterized by the formation of nuclei of FeO, CO (or CO_2) and a small amount of Al_2O_3. CO (or CO_2) gas then evaporates and goes into the environment from the surface of the specimen. As the growth rate of FeO is more rapid than that of Al_2O_3, this results in iron oxide overgrowing the Al_2O_3. As the oxidation time gets longer, $FeFe_xAl_{2-x}O_4$ is suggested to be formed by the chemical reaction between FeO and Al_2O_3. Generally, CO (or CO_2) gas is transported through the pores and microcracks of the oxide scale. As oxidation proceeds, Fe_3O_4 and Fe_2O_3 are formed as an external layer and a fine dispersion of Al_2O_3 and discontinuous layers of $FeFe_xAl_{2-x}O_4$ are established along the oxide–metal interface.

The initial oxidation rate is the lowest one among the three distinct parabolic laws that are observed from our oxidation experiments carried out at 800° C for 24 h. Generally, the first stage of oxidation lasts about 3 h and the second stage lasts from 3 to 10 h with an oxidation rate higher than the initial one. However, the third oxidation rate is slightly lower than the second one (Table II). According to the metallographic studies using an optical microscope, the oxidation of the Fe–5.5 Al–0.55 C alloy at 800° C was always accompanied by decarburization of the
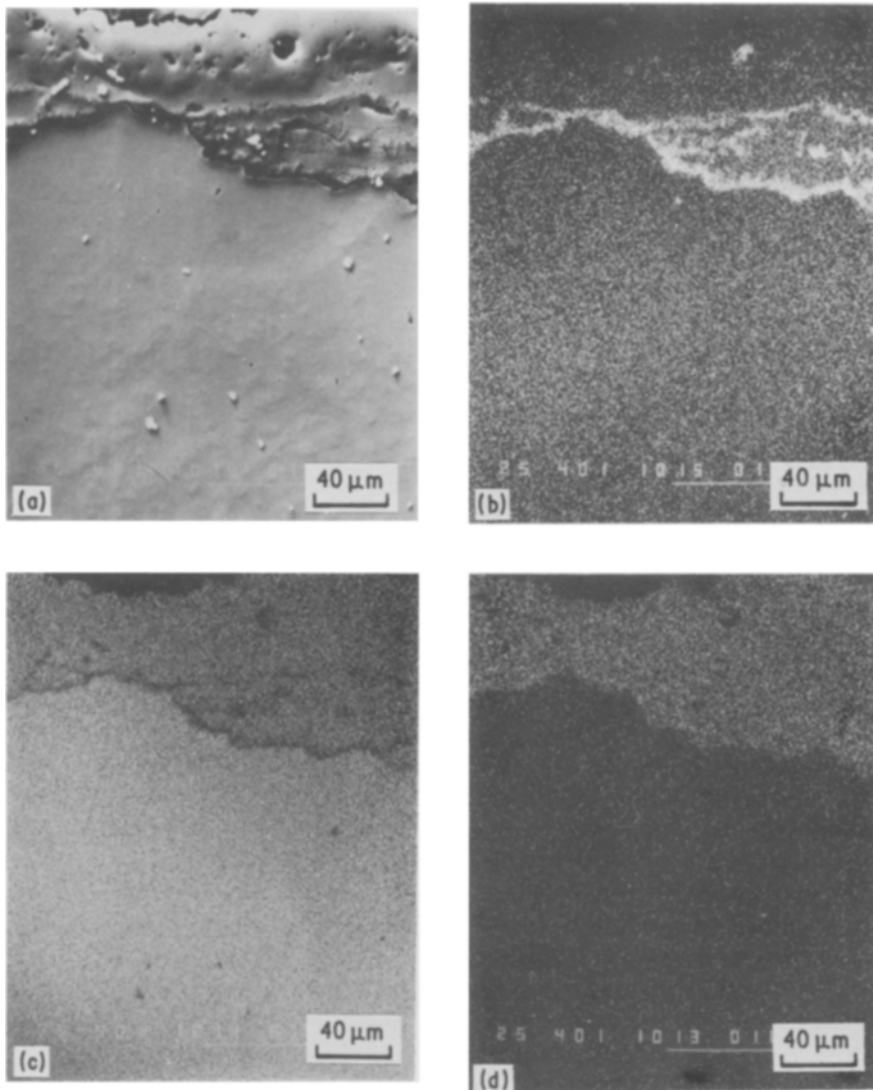

Figure 7 Metallographic cross-section of nodules on Fe–5.5 Al–0.55 C alloy after 1 h at 1000° C.

3206

Figure 8 Scanning electron micrograph of the oxide scale on Fe–5.5 Al–0.55 C alloy at 1000° C after 2 h: (a) SEM picture, (b) X-ray map for aluminium, (c) X-ray map for iron, (d) X-ray map for oxygen.

substrate. A carbide-free layer was generally observed just below the oxide–metal interface, but no protective aluminium oxide film could be found. The thickness of such a layer increased as the oxidation time increased. For a better understanding of the formation of this carbide-free layer, the stability of carbide particles at 800° C was checked by holding a

piece of the present alloy at 800° C for two hours and then quenching into water at room temperature. An obvious size and volume fraction change of these carbide particles indicated that the carbide particles were at least partially decomposed at 800° C. The remaining carbide should have been in thermodynamic equilibrium with the carbon concentration in the
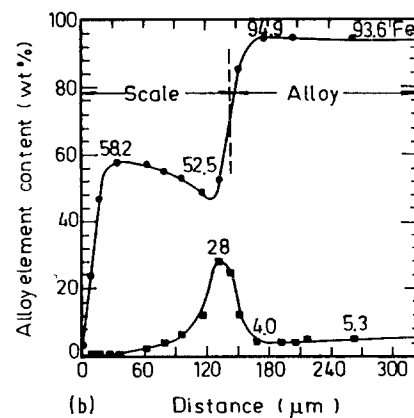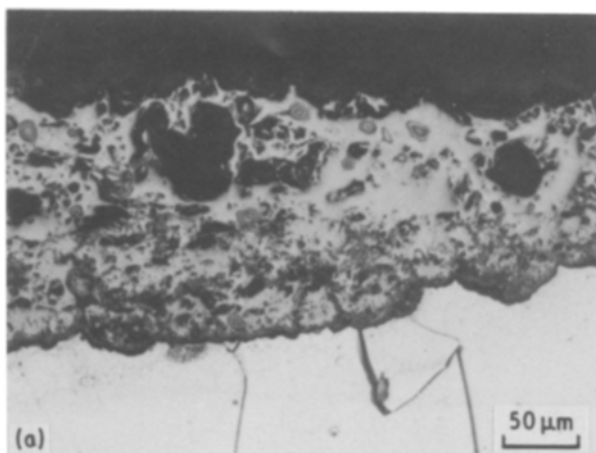

Figure 9 (a) Metallographic cross-section of oxide scales on Fe–5.5 Al–0.55 C alloy after 24 h at 1000° C. (b) The concentration profile across the line marked in (a).

3207

surrounding region, where carbon atoms came from decomposed carbide particles. Under such conditions, in the region closest to the surface the carbon concentration decreased more rapidly as the carbon atoms diffused out and reacted with oxygen and finally evaporated. This made the carbide particles lose their stability and kept the decomposition continuously going, so that finally the carbide particles totally disappeared from this region. On the other hand, no decarburized zone appeared when the alloy was oxidized at 600° C. Such differences were evident not only in the micrographs observed from the cross-sections of oxidized specimens but also in the kinetic data.

It was found that the oxidation rate of the Fe–5.5 Al–0.55 C alloy was observed to be higher than that of Fe–5 Al alloy at 800° C. Kinetic studies combined with morphology investigations demonstrated that the largest portion of the oxide scales was occupied by iron oxide nodules (Fig. 6), and the weight gain of the oxidized specimens was mainly from the formation of such nodules. A similar result was also reported by Boggs [7].

The deviation of the slope observed in Fig. 3b might be due to the evolution of CO or CO_2 in the secondary stage of oxidation, suggesting that the formation of CO or CO_2 at the alloy–oxide interface may rupture the oxide layer and therefore change the kinetics of the oxidation process. However, the possibility that the evolution of carbon monoxide (and/or carbon dioxide) might exert an effect on the oxidation of the alloy cannot be excluded. This evolution of gas would hinder, to some extent, the formation of protective oxide layers, and produce cracks and blisters [8].

As the oxidation experiment at 800° C was carried out, carbide atoms which mostly came from the decomposition of carbide particles diffused out to the specimen surface and evaporated with the formation of CO (or CO_2). This made the carbon concentration in the alloy decrease as oxidation progressed. When the carbon content fell to a certain level, evolution of CO (or CO_2) gas could have been restricted so as to lead to the start of the third stage of oxidation, which always had a lower oxidation rate than the secondary stage of oxidation.

The kinetic curve obtained from oxidation experiments at 1000° C appears to be different from those for 600 and 800° C. It indicates that there are two distinct parabolic laws for the present alloy at 1000° C. Based on the results of optical observations, iron–aluminium carbide (Fe_3AlC_x) was not found in the alloy after one hour of oxidation. It is believed that the rate of diffusion of carbon in the alloy at 1000° C is higher than at 800° C. This would make the specimen surface of the alloy to be covered by nodular scales much more rapidly. The initial parabolic rate of the alloy for oxidation at 1000° C is higher than that at 800° C (Table II).

From the results of optical morphology, X-ray mapping and X-ray diffraction investigations, the oxide scales observed on the Fe–5.5 Al–0.55 C alloy after 24 h oxidation at 1000° C consisted of a mixture of iron and aluminium oxide. $FeAl_2O_4$ was always found along the oxide–metal interface. It therefore seems that the formation of $FeAl_2O_4$ scale occurred at the final stage and hercynite began to predominate. Thus, as the temperature increases, and the mobility of aluminium atoms in the alloy increases, more and more aluminium in $FeFe_xAl_{2-x}O_4$ ($0 \leqslant x \leqslant 2$) was formed, and the final oxidation rate dropped.

5. Conclusions

1. The high-temperature oxidation behaviour of Fe–5.5 Al–0.55 C varied as the oxidation experiments were carried out at 600, 800 and 1000° C in air.

2. During the oxidation of the alloy at 600° C, a simple parabolic law was observed. There are three distinct parabolic rates and two distinct parabolic rates for the alloy at 800 and 1000° C, respectively.

3. No carbide-free layer could be observed in specimens of Fe–5.5 Al–0.55 C alloy after 24 h oxidation at 600° C. A partial dissociation of carbide was found for the present alloy during oxidation at 800° C. Carbide quickly dissociated in the matrix when the specimen was oxidized at 1000° C.

4. Decarburization had a harmful effect on the oxidation resistance in this study.

Acknowledgement

References

1. E. R. MOGAN and V. F. ZACKAY, *Metal Prog.* **90** (1955) 126.
2. D. J. SCHMATZ, *Trans. ASM* **52** (1960) 898.
3. J. L. HAM and R. E. CAIRNS Jr, *Prod. Engng* **29** (1958) 50.
4. J. C. GARCIS, N. ROSAS and K. RIOJA, *Metal Prog.* **117** (1982) 47.
5. C. H. KAO, C. M. WAN and M. T. JAHN, in Proceedings of Symposium on Alternate Alloying for Environmental Resistance, New Orleans, March 1986, in press.
6. F. SAEGUSA and L. LEE, *Corrosion* **22** (1966) 168.
7. W. E. BOGGS, *J. Electrochem. Soc.* **118** (1971) 906.
8. W. W. WEBB, J. T. NORTON and C. WAGNER, *ibid.* **103** (1956) 112.